Laser-Induced Forward Transfer of Ni-rich NiTi Alloys for Shape Memory Applications

Logaheswari Muniraj[*1], Marcus Ardron[2], Robert L Reuben[3], and Duncan P Hand[1]

[1]*Institute of Photonics and Quantum Sciences, Heriot-Watt University, Edinburgh, EH14 4AS, UK*
[2]*Renishaw Plc., Research Avenue, Edinburgh, EH14 4AP, UK*
[3]*Institute of Mechanical, Process, and Energy Engineering, Heriot-Watt University, Edinburgh, EH14 4AS, UK*
[*]*Corresponding author's e-mail: llm5@hw.ac.uk*

Laser-induced forward transfer (LIFT) is a direct-write technique that uses laser pulses to sequentially deposit small volumes of a material from one substrate to another. It is a proven deposition process to fabricate complex functional micro-structures. Shape memory alloys (SMAs) are active materials that can be deformed at low temperatures and return to their original parent shape under the influence of appropriate thermomechanical conditions (i.e. by changing the temperature and/or the stress). Functional grading of SMA characteristics by precisely controlling the composition locally can provide a complex actuation response of the overall structure to external stimuli (stress, temperature) thereby significantly widening applications. Conventionally, SMAs are bulk heat-treated during the manufacturing process to ensure homogenization, eliminate internal defects, and, by implication, alter transformation temperatures. High power lasers can provide localized heating coupled with high heating and cooling rates, and hence provide the opportunity to control the formation of microstructures and the resulting phase, but this technique has not yet been fully explored with SMAs. In this paper, we explored this potential by fabricating NiTi based alloys using LIFT and then subjecting them to heat treatment using a nanosecond laser.
DOI: 10.2961/jlmn.2023.02.2007
Keywords: laser direct-write, LIFT, shape memory alloys, heat treatment, micro-actuators.

1. Introduction

Shape memory alloys (SMAs) are materials that have a unique crystallographic structure, centered around an austenite-martensite transformation[1] that provides them with the ability to undergo a "shear transformation" when subjected to appropriate thermal or stress conditions (Shape Memory Effect (SME)). During this process, these alloys can generate high actuation energy densities (available work output per unit volume) making them suitable candidates for the fabrication of actuators[2]. Micro-scale actuators are particularly a interesting as they possess a strong advantage to generate large force within a small volume. They could be integrated in the field of micro-electromechanical systems (MEMS) to fabricate energy harvesting devices[3], mass, force, and temperature sensors[4] and Lab-on-a-Chip systems[5]. However, the lack of specialized fabrication techniques and design tools, coupled with technological barriers to produce spatially functioning devices with high resolution and composition control currently limits their applications.

Nickel-titanium (NiTi) based SMAs are widely used in biomedical applications owing to their attractive features such as biocompatibility, high corrosion resistance, high fatigue strength and a transition temperature close to body temperature making them suitable candidates to fabricate in-vivo actuated medical devices. Some of the well-known examples of these devices include cardiovascular stents[6], micropumps, micro-grippers[7], and micro-endoscopes[8]. Most often these alloys are manufactured by casting, powder metallurgy or vapor deposition techniques[9] which do not provide spatial or compositional control for complex structures beyond wires and sheets. Our approach is to use a laser driven process to fabricate NiTi based micro-actuators by precisely and locally controlling their elemental composition and thereby produce a more complex response to temperature. Functional grading (locally changing the composition and hence the shape memory transition temperature) of NiTi has the potential to provide sufficient control to manipulate an SMA actuator response to stress and temperature by widening their transformation window[10].

Laser-induced forward transfer (LIFT) was introduced by Bohandy *et. al*[11] in 1986 who used the technique to produce micron sized deposits of copper using a thin copper film. Since then, many different variations of the technique have been used to fabricate 3D micro-structures[12], high aspect ratio pillars[13], and alloying of multiple layers of metals[14]. LIFT uses either short (nanosecond) or ultrashort (pico- or femtosecond) pulses to print structures by ejecting either a melt or solid from a thin film on a donor substrate. A minimum feature size of 330 nm has been demonstrated with 110 fs pulses, as reported by Banks *et al.*[15]. Gorodesky *et al.* studied the phase, structure, and composition of LIFT printed Cu-Ag and reported on the high cooling rates associated with the LIFT process that produces amorphous deposits[16]. This paper also shows that most structures printed by LIFT require additional heat treatment to induce recrystallization and grain growth. Bulk SMAs are generally subjected to specific thermo-mechanical treatments[17] to strengthen their mechanical properties, achieve

final shape setting or manipulate the transformation temperature. Laser-based annealing processes are more commonly used in NiTi thin films to locally modify the SMA behavior by selectively crystallizing particular areas[18] or improve their corrosion resistance[19]. Reported studies on the impact of heating on the microstructure and phase transformations of NiTi SMAs are mostly limited to conventional heat treatment methods such as annealing in a furnace at a specific temperature for prolonged durations to homogenize the alloy. Recently, laser-based additive manufacturing methods have been used to produce NiTi SMAs, where a key challenge is the control of the localized heating and rapid cooling to avoid the formation of undesired phases and intermetallic compounds[20]. By tailoring the laser parameters, the porosity, hardness, and shape memory characteristics of the SMA can be tuned.

In this work, we use LIFT to fabricate Ni-rich NiTi deposits, using femtosecond pulses from an IR laser to print deposits from a thin NiTi donor film pre-deposited onto a microscope slide. The influence of the laser parameters on the printed NiTi before and after heat treatment using an IR laser with a pulse width of 350 ns was assessed using microscopical/morphological and SEM-EDX analysis.

2. Experiment

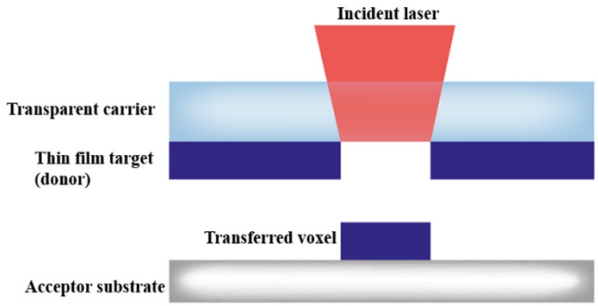

Fig 1 Schematic of LIFT setup with all the main elements for laser printing. A pulse from the incident laser is focused on the glass-thin film interface.

LIFT transfer of metals usually requires a thin film of metal on a transparent substrate (glass, quartz) that acts as a donor. We use a thin film coating (200 nm) on a microscope slide (75×25×1 mm) supplied by Teer coatings made by magnetron sputtering using a NiTi target (50:50 at. %)[21]. The receiver for the preliminary parameter optimization is a conventional microscope glass substrate. For the characterization of morphology and composition after heat-treatment, we used a silicon substrate (10×10 mm).

The laser used in our LIFT experimental setup is a diode-pumped ultrafast laser (Tangerine, Amplitude Systèmes). It has a wavelength of 1030 nm, pulse duration of 260 fs and a Gaussian intensity profile (M^2 < 1.3). The output beam is expanded 3× using a beam expander telescope and is further directed onto a 2-axis galvanometer scan head (Lasea LS-Scan). The F-theta lens (167 mm focal length) focusses the laser beam to a calculated spot diameter of 27 µm ($1/e^2$) at the interface in between the front surface of the NiTi thin film and back surface of the glass substrate, Fig 1, shows the schematic of the LIFT system. The distance between the donor and receiver substrate was set to 10 µm.

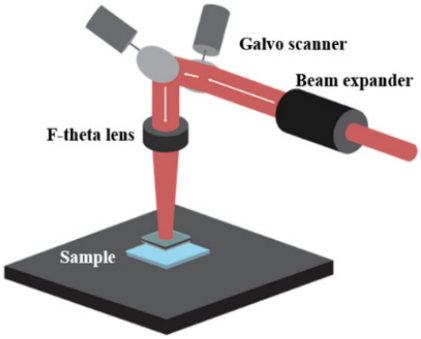

Fig 2 Schematic representation of LIFT setup. The laser is focused onto the donor film via a galvo scanner and F-theta lens. This allows the beam to be rapidly scanned and hence large areas of LIFT can be generated.

A single deposit is obtained for every pulse when the applied fluence is slightly higher than the transfer threshold. The quality of the deposit depends on the fluence, thickness of the film and donor film diffusion length [22]. A galvo scanner is used to direct the laser pulses, Fig 2, and hence generate high resolution 3D microstructures, Figure 3, by choosing a suitable laser scan speed, repetition frequency and hatch spacing (i.e., the spacing between adjacent scan lines). Using high precision linear stages, the donor or the receiver substrate can be translated in the z direction (keeping the distance between the substrate and the deposit constant). This will allow us to fabricated 3D structures using the optimized laser parameters.

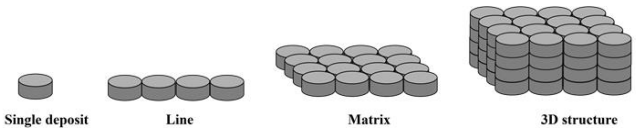

Fig 3 Structuring of LIFT deposits.

Subsequent heat treatment of the resulting deposited material is carried out using a pulsed fibre laser from SPI (20 W EP-S) that has a wavelength of 1064 nm. The light from the laser is fibre delivered to a beam expander collimator that directs it into a galvanometer scan head (RLA-1504 [Y] D2) that is focused onto the surface of the deposited NiTi grid on the silicon substrate. The diameter of the laser spot is calculated to be 63 µm ($1/e^2$). This nanosecond fibre laser provides us 39 different pulse 'waveforms' each corresponding to a different pulse length (3-490 ns)[23]. We used a pulse width of 350 ns for heat treating our NiTi deposits. The laser beam is scanned across the deposited material following a raster scan strategy with a repetition frequency of 332 kHz and scan speed of 250 mm/s, to provide a pulse overlap of 98% and a hatch overlap of 77%. The sample is placed on Z-axis stage inside a gas chamber with constant argon flow during the process to prevent the formation of oxides.

The deposited structures are imaged using a Leica microscope (DM6000M). The surface profile of the matrices is characterized using an Alicona surface profilometer (InfiniteFocus, Alicona Imaging GmbH). The compositions of the printed layers are measured using energy dispersive X-ray spectroscopy (EDS) in combination with a Scanning electron microscope (Tescan VEGA) analysis.

3. Results and discussion

Firstly, the fluence for optimum deposition of NiTi deposits is obtained by printing at increasing fluences. This is further extended to printing grids by optimizing laser scan speeds and hatch spacing. The printed grids are then heat-treated using ns-pulses to activate surface recrystallization and grain growth. The resulting micro-structure and composition is obtained using SEM-EDX analysis.

3.1. LIFT printing of NiTi

As the fluence is increased from 0.3 J/cm^2 to 5.2 J/cm^2 the deposit morphology changes significantly, see Fig 4. The threshold fluence for transfer was estimated to be 0.3 J/cm^2 since below this value no deposits could be seen. The minimum size of the deposit obtained was 4 µm. Slightly above the transfer threshold, larger deposits close to the width of the focused laser spot are obtained. These deposits are significantly larger at higher intensities due to spreading of the main deposit coupled with formation of spatter or debris around the main deposit.

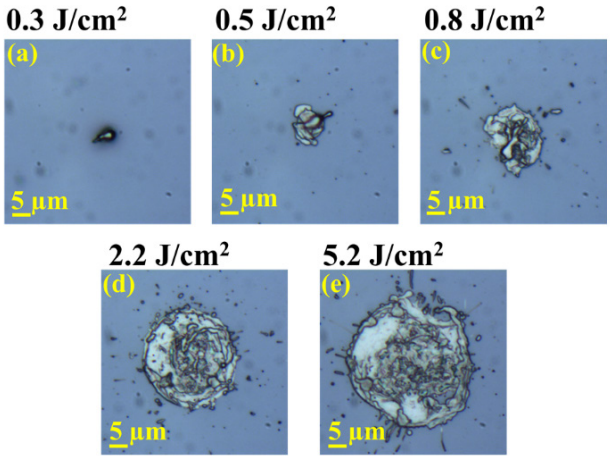

Fig 4 Optical microscopy images of NiTi deposits as a function of fluence: (a) 0.3 J/cm^2, (b) 0.5 J/cm^2, (c) 0.8 J/cm^2, (d) 2.2 J/cm^2 and I 5.2 J/cm^2.

Since our approach is to produce NiTi layers from an array of deposits, it is essential to choose a deposit that is flat and fully filled. This means that the volume of the deposit (and hence the composition) can be readily estimated, and that stacking can be used to increase its thickness. Close to the process threshold, Fig 4(a) and (b), the ejection of a droplet to produce controlled deposits is heavily dependent on the differences in surface tension, melt viscosity and velocity of ejection making it difficult to predict the droplet position and size. The deposits obtained at 0.8 J/cm^2, Fig 4(c), have quite random shapes whilst, for fluences above 2.2 J/cm^2, Figure 4(e), the deposits are quite circular but not fully filled. At 2.2 J/cm^2 the deposit is close to a symmetric circle (diameter 24 µm) and the debris are minimal making this fluence a good choice for building larger structures. It is also worth noting that the fluence required for obtaining deposits using an amorphous thin film is much less than that required for from a crystalline film[14], [24] . This may be due to the inter-atomic bonds that exist between the film and the substrate surface. Low fluences, therefore, help to produce highly reproducible deposits with good shape preservation. Fig 5 shows optical microscope images of NiTi lines printed at scan speeds varying from 350 mm/s to 50 mm/s at a laser repetition frequency of 10.29 kHz and a fluence of 2.2 J/cm^2. The distances between the deposits relates to the scan speed (v) and repetition frequency (f) given by $\Delta S = v/f$. At lower scan speeds, the laser pulses on the donor thin film start overlapping each other hindering the ejection of the droplet and thus ruining the formation of the deposit, Fig 5(g). At higher scan speeds, the lines are not continuous, but the individual deposits are identical to each other and are in the expected positions, Fig 5(a). It can be seen that the optimum scan speed is 250 mm/s, Fig 5 4(c), where each pulse contributes to a fully formed deposit without any overlapping. After optimizing the scan speed, the hatch distance was set equal to the distance between the pulses (24 µm) at 250 mm/s.

3.2. Laser-based heat treatment

The lines are printed together in series to produce a NiTi layer of size 5 mm × 5 mm on a silicon substrate. Fig 6 shows the optical microscope image of the NiTi grid at 10× magnification and the inset shows the deposits at 100× magnification. In terms of deposit morphology, the deposits obtained on glass, Figure 4, and silicon are of similar size and shape.

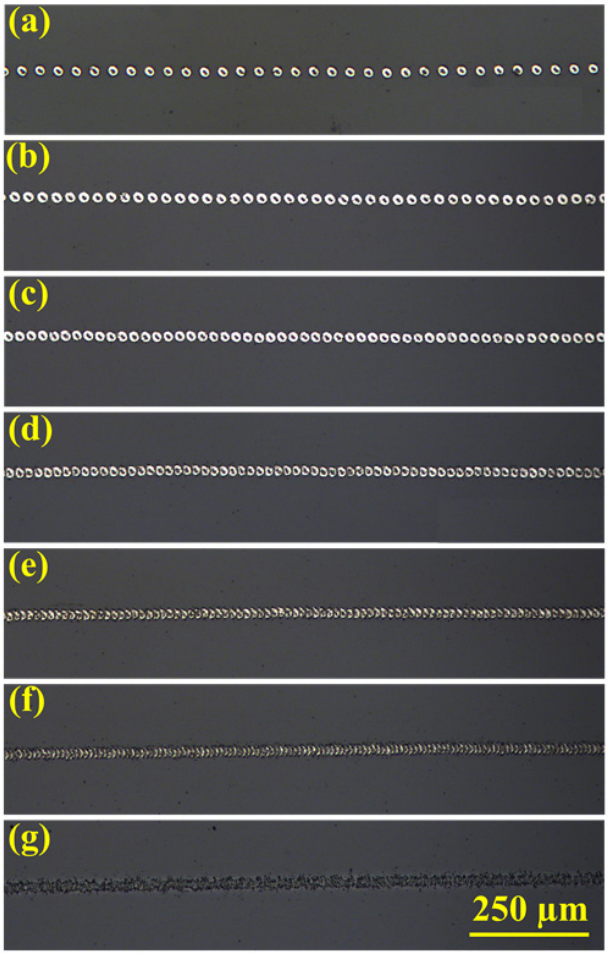

Fig 5 LIFT printed deposits at decreasing scan speeds: (a) 350 mm/s, (b) 300 mm/s, (c) 250 mm/s, (d) 200 mm/s, (e) 150 mm/s, (f) 100 mm/s, (g) 50 mm/s.

Nevertheless, we observe a decrease in the number of splatters when deposited on silicon, attributed to the thin oxide layer that provides the necessary adhesion to produce

better deposits. It can be observed that the individual deposits are placed accurately close to each other without any interruptions showing the reproducibility of the droplet deposition.

Each 5 mm line consists of 210 deposits and the printing of an entire 5 mm × 5 mm takes only about 10 seconds. Although the deposits are consistently placed there are small interstitial gaps caused by the circular shape. To produce a uniform layer for heat treatment, three layers of the NiTi grid are stacked on top of each other with a small offset.

Fig 7(a) shows an optical microscope image of three LIFT-printed layers of NiTi. Subsequent layers were offset to fill the interstitial gaps, and the root mean square (RMS) height of the top surface was measured to be 562 nm whereas that of a single layer was 142 nm. The energy dose deposited per area (J/mm^2) was calculated using $E = E_P/(\Delta S.\Delta H)$ where E_P is the pulse energy (J), ΔS is the scan spacing (mm), and ΔH is the hatch spacing (mm).

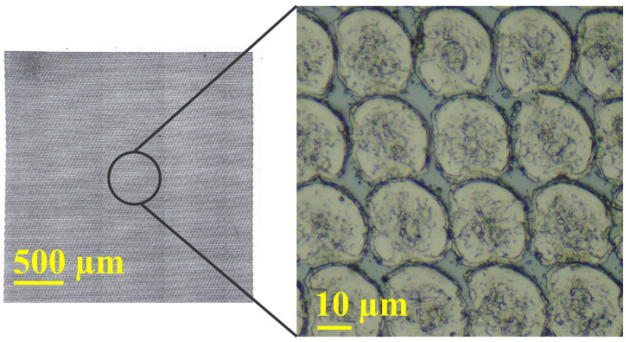

Fig 6 Optical microscope images of 5 × 5 mm LIFT-printed NiTi array grid.

At 1.7 J/mm^2, Fig 7(b), the NiTi layer begins to melt redistributing the deposits and hence making the surface uniform. The laser tracks are clearly visible at 2.1 J/mm^2, Fig 7(c), with some distinct features near the hatch spacing, most likely due to the Gaussian energy distribution of the spot. Using higher energy doses, Fig 7(d), the surface reaches higher temperatures causing a prolonged melt duration resulting in less distinct laser track borders.

Table 1 Chemical composition EDS results of heat treated NiTi matrix at 2.8 J/mm^2 (Figure 8)

Spectrum (At. %)	Ni	Ti
1	55	44
2	55	44
3	54	45
4	56	43
5	54	45

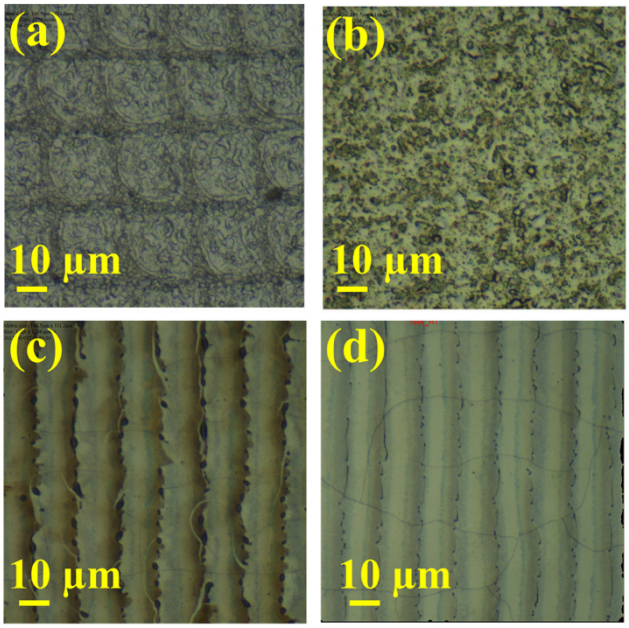

Fig 7 Optical microscope image a) Three layers of NiTi matrix heat treated at b) 1.7 J/mm^2, c) 2.1 J/mm^2, d) 2.8 J/mm^2.

Table 1 shows the composition of the donor thin film, together with LIFT-printed layers and the heat-treated layer at 1.7 J/mm^2, measured at 3 random points in each case, using the EDX-SEM. The donor thin film is (unexpectedly) Ni-rich NiTi, with 56 at. % of nickel. The LIFT printed layer and heat-treated layer have slightly lower nickel content attributed to loss of some material during ejection and influence of laser pulses on the surface of the matrix. Fig 8(a) shows the SEM image of the heat-treated surface at 2.1 J/mm^2. There are large cracks formed perpendicular to the laser scan pattern, most likely solidification cracks due to the temperature gradient below the spot and/or the difference in thermal expansion coefficients and elastic modulus of the NiTi matrix and the silicon substrate[25]. On heating close to the melting point, nickel-rich Ni-Ti alloys go through an L (liquid) + NiTi phase field and so will produce some Ni-rich liquid prior to general melting. Fig 8(b), (c), (d) show some nickel rich pockets on top of titanium rich protrusions implying that the maximum surface temperature is not quite high enough for general melting in some places. Outside the titanium rich protrusions and nickel rich pockets, the surface is filled with darker and lighter patches visible in the back-scattered electron image. The dark regions correspond atomically to a Ni-rich intermetallic compound (Ni_4Ti_3) again probably caused by short-term exposure at high sub-melting temperatures. At even higher energy doses (2.8 J/mm^2), Fig 8(b) and Fig 7(d), the as-deposited surface has a more polished appearance, suggesting more general melting and the surface no longer has nickel or titanium rich patches. The dot spectra obtained on random positions, Fig 9, on the surface (Table 2) have similar atomic composition throughout corresponding to Ni-rich NiTi as for the donor film (Table 1).

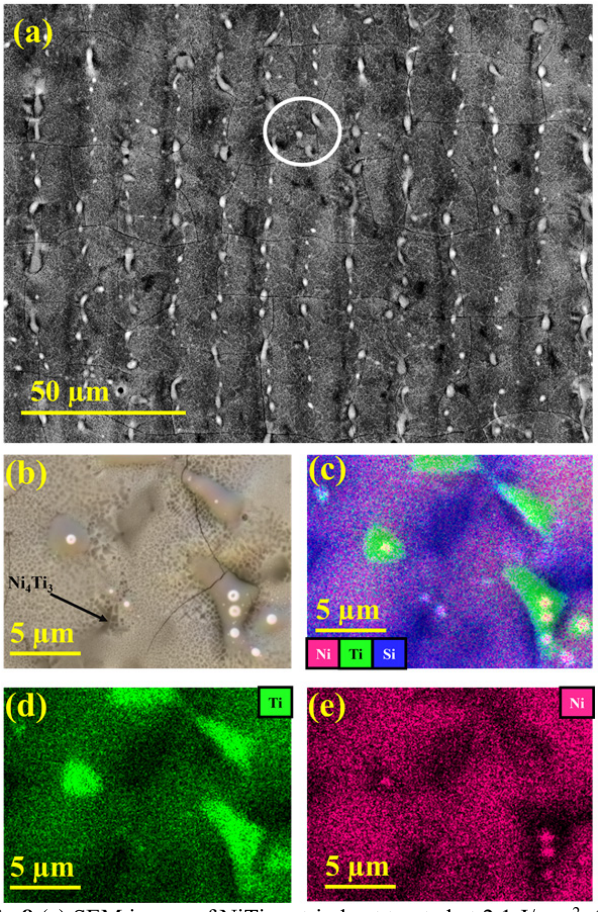

Fig 8 (a) SEM image of NiTi matrix heat treated at 2.1 J/mm^2, (b) magnified SEM (backscattered electrons) image of the surface, (c) EDX layered image with Ni (pink), Ti (green) and silicon substrate (blue) mapping, (d) Ti map, (e) Ni.

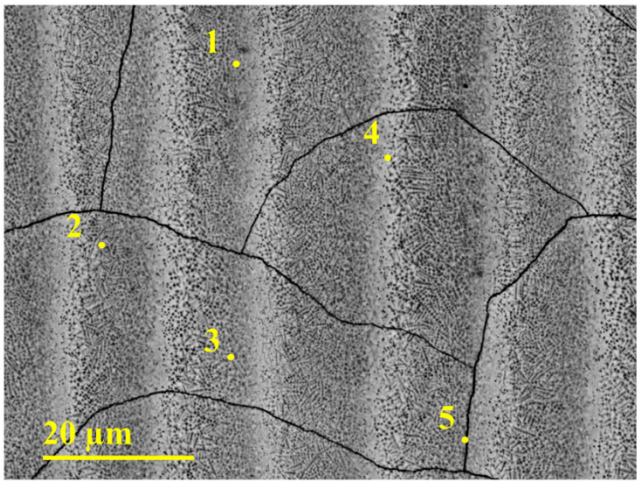

Fig 9 SEM image of heat treated NiTi matrix at 2.8 J/mm^2, dot spectra obtained at random locations. At %. of the various spots are given in table 2.

Small variations in the chemical composition of equiatomic NiTi induces large variations in the transformation temperatures. An increase of 0.1 at. % is known to decrease the transformation temperature by 10 K [26]. It is expected that these deposits would function as a shape memory alloy, however, with large shifts in transformation temperature induced by the excess nickel and additional intermetallic compounds.

Table 2 Chemical composition EDS results

Spectrum (At. %)	Donor thin film		LIFT printed layer		HT layer at 1.7 J/mm^2	
	Ni	Ti	Ni	Ti	Ni	Ti
1	56	43	55	44	57	42
2	56	43	54	45	56	43
3	56	43	55	44	55	44

4. Conclusions

This work demonstrates the feasibility of using laser-based techniques for fabrication and heat treatment of NiTi SMA micro-structures, specifically:

- LIFT of amorphous thin films using lower fluences allows us to deposit good quality, reproducible structures which can be built up in a “pointillist” fashion.
- Laser-based heat treatment provides intricate control of the thermal cycle experienced by the LIFT-deposited material to control the constitution (phase distribution) of the alloy.
- There is always a risk of producing undesired phases which compromise of mechanical properties of the layers. This can be avoided by further process optimization and control of the different laser parameters.
- We have demonstrated the transfer of a slightly nickel-rich NiTi with good compositional fidelity.
- We have demonstrated that we can control the temperature in the surface layer to achieve surface melting without fusion of the underlying substrate.
- This work forms the basis of a future laser-based manufacturing process for fabrication of miniature tailored SMA structures.

References

[1] G. Kostorz: "Phase transformations in materials", (Wiley, New York, 2001) p.641.

[2] Dimitris C. Lagoudas: "Shape Memory Alloys: Modeling and Engineering Applications", Boston, MA: (Springer US, 2008) p.2.

[3] H. Liu, J. Zhong, C. Lee, S.-W. Lee, and L. Lin: Appl. Phys. Rev., **5**, (2018) 041306.

[4] Y. Fu, H. Du, W. Huang, S. Zhang, and M. Hu: Sens. Actuators Phys., **112**, (2004) 395.

[5] C. H. Ahn and J.W. Choi: "Microfluidics and Their Applications to Lab-on-a-Chip" ed. by B. Bhushan in (Springer Handbook of Nanotechnology, 2004) p.253.

[6] S. Omid, Z. Goudarzi, L. Kangarshahi, A. Mokhtarzade, and F. Bahrami : J. Compos. Compd., **2**, (2020) 92.

[7] H. Mehrabi and I. Aminzahed: Microsyst. Technol., **26**, (2020) 531.

[8] E. Makino, T. Mitsuya, and T. Shibata: Sens. Actuators Phys., **88**, (2001) 256.
[9] M. A. Zainal, S. Sahlan, and M. S. M. Ali: Micromachines, **6**, (2015) 879.
[10] Shariat, Bashir S., et al. : Materials and Design., **124**, (2017) 225.
[11] J. Bohandy, B. F. Kim, and F. J. Adrian : J. Appl. Phys., **60**, (1986) 1538.
[12] M. Feinaeugle, R. Pohl, T. Bor, T. Vaneker, and G. Römer: Addit. Manuf., **24**, (2018) 391.
[13] M. Zenou and Z. Kotler: Opt. Express, **24**, (2016) 1431.
[14] L. Muniraj, B. Siwicki, M. Ardron, D. P. Hand, and R. L. Reuben: Proc. SPIE, Vol.11988, (2022).
[15] D. P. Banks, C. Grivas, J. D. Mills, R. W. Eason, and I. Zergioti: Appl. Phys. Lett., **89**, (2006) 193107.
[16] Gorodesky, N., Sedghani-Cohen, S., Fogel, O., Altman, M., Cohen-Taguri, G., Kotler, Z. and Zalevsky, Z: Adv.Eng.Materials., **24**, (2022) 2100952.
[17] D. Treppmann, E. Hornbogen: Journal de physique., **7**, pp. 211-220, (1997).
[18] X. Wang, Y. Bellourd, J.J. Vlassak: Acta Materialia., **53**, (2005) 4955.
[19] F. Villermaux, M. Tabrizian, L. Yahia, M. Meunier, and D. L. Piron: Appl. Surf. Sci., **109,** (1997) 62.
[20] J. J. Marattukalam, V. K. Balla, M. Das, S. Bontha, and S. K. Kalpathy: J. Alloys Compd., **744**, (2018) 336.
[21] J. Rao, T. Roberts, K. Lawson, and J. Nicholls: Surf. Coat. Technol., **204**, (2010) 2331.
[22] P. Serra and A. Piqué: Adv. Mater. Technol., **4** , (2018) 2100952.
[23] S. D. Dondieu *et al.*: J. Manuf. Mater. Process., **4** , (2020) 110.
[24] N. Gorodesky *et al.*: Crystals, **11**, (2021) 291.
[25] Z. Yu *et al.*: Chin. J. Mech. Eng., **34**, (2021) 92.
[26] J. Frenzel, Z. Zhang, K. Neuking, and G. Eggeler: J. Alloys Compd., **385**, (2004) 214.

(Received: June 16, 2023, Accepted: September 5, 2023)